Bifunctional Magnetic Silica Nanoparticles for Highly Efficient Human Stem Cell Labeling

Chen-Wen Lu,[†] Yann Hung,[‡] Jong-Kai Hsiao,[§] Ming Yao,[||] Tsai-Hua Chung,[†]
Yu-Shen Lin,[‡] Si-Han Wu,[‡] Szu-Chun Hsu,[||] Hon-Man Liu,[§] Chung-Yuan Mou,[‡]
Chung-Shi Yang,[⊥] Dong-Ming Huang,*,[⊥] and Yao-Chang Chen[†,||]

*Center for Nanomedicine Research and Stem Cell Research Center, National Health
Research Institutes, Miaoli 350, Taiwan, Department of Chemistry, National Taiwan
University, Taipei 112, Taiwan, and Department of Laboratory Medicine and
Department of Medical Imaging, National Taiwan University Hospital and College of
Medicine, Taipei 112, Taiwan*

Received October 16, 2006; Revised Manuscript Received November 20, 2006

ABSTRACT

A superparamagnetic iron oxide (SPIO) nanoparticle is emerging as an ideal probe for noninvasive cell tracking. However, its low intracellular labeling efficiency has limited the potential usage and has evoked great interest in developing new labeling strategies. We have developed fluorescein isothiocyanate (FITC)-incorporated silica-coated core−shell SPIO nanoparticles, $SPIO@SiO_2(FITC)$, with diameters of 50 nm, as a bifunctionally magnetic vector that can efficiently label human mesenchymal stem cells (hMSCs), via clathrin- and actin-dependent endocytosis with subsequent intracellular localization in late endosomes/lysosomes. The uptake process displays a time- and dose-dependent behavior. In our system, $SPIO@SiO_2(FITC)$ nanoparticles induce sufficient cell MRI contrast at an incubation dosage as low as 0.5 μg of iron/mL of culture medium with 1.2×10^5 hMSCs, and the in vitro detection threshold of cell number is about 1×10^4 cells. Furthermore, 1.2×10^5 labeled cells can also be MRI-detected in a subcutaneous model in vivo. Labeled hMSCs are unaffected in their viability, proliferation, and differentiation capacities into adipocytes and osteocytes which can still be readily MRI detected. This is the first report that hMSCs can be efficiently labeled with MRI contrast nanoparticles and can be monitored in vitro and in vivo with a clinical 1.5-T MRI imager under low incubation concentration of iron oxide, short incubation time, and low detection cell numbers at the same time.

To monitor cell trafficking in vivo and distinguish whether cellular regeneration originated from an exogenous cell source is a key issue for developing successful stem cell therapies. Most of the traditional techniques for the examination of stem cell transplantation in animal models are performed by postmortem histological analysis.[1−3] Obviously, these histological methods cannot be applied in clinical studies. Thus, it is important to develop methods that can monitor the fate and distribution of transplanted stem cells noninvasively. Magnetic resonance imaging (MRI) is an ideal imaging modality for the biodistribution of magnetically labeled cells.[4−12] For MRI detection, cells need to be internally labeled with MRI contrast agents. Although native superparamagnetic iron oxide (SPIO) particles appear currently to be the preferred cell-labeling materials,[3] they suffer from low intracellular labeling efficiency. Hence, more efficient cellular-internalizing methods are highly desirable. Several modifications of SPIO particles, including coating with polystyrene, dextran, and dendrimer and utilizing of other transfection agents, have been reported to improve internalization of the contrast agent. However, the internalizing efficiency is still generally low as manifested by the requirement of a long-term incubation or a high concentration of particles with cells.[5,6,8,9,12] An alternative strategy to improve internalizing efficiency is to link the particles to a HIV tat peptide or monoclonal antibody.[4] Although these peptides efficiently transport the iron oxide particles into cells, the key issue regarding the biosafety of a xenogeneic protein should be seriously considered. Especially for stem cell tracking, the biological effects of the internalized particles surely have higher priority over other considerations including the cellular labeling efficiency. Furthermore, in order to compensate for the limited MRI sensitivity due to

* Corresponding author. Dong-Ming Huang. Center for Nanomedicine Research, National Health Research Institutes, 35 Keyan Rd, Zhunan, Miaoli 350, Taiwan, R.O.C.; tel, 886-37-246-266 ext.38105; fax, 886-37-586-447; e-mail, dmhuang@nhri.org.tw.
† Stem Cell Research Center, National Health Research Institutes.
‡ Department of Chemistry, National Taiwan University.
§ Department of Medical Imaging, National Taiwan University Hospital and College of Medicine.
|| Department of Laboratory Medicine, National Taiwan University Hospital and College of Medicine.
⊥ Center for Nanomedicine Research, National Health Research Institutes.

the low intracellular labeling efficiency, previous studies were usually performed on MRI systems with higher field strength[4,6,8,9] than most clinical MRI imagers of 1.5 T. Some other reports employed large numbers of cells for 1.5-T MRI imagers.[10−12]

Recently, bifunctional contrast agents with both optical and magnetic contrast were demonstrated to serve as good molecular imaging probes both in vitro and in vivo.[13,14] Thus, dual-modality detections could be simultaneously achieved using a single material. In our synthetic strategy, silica (SiO_2) was selected for surface coating of SPIO particles because dye molecules can be easily incorporated into a silica shell, and silica is quite biocompatible and resistant to biodegradation in the biological environments.[15,16] Moreover, silica can be easily surface functionalized for bioconjugation and targeting for various applications in biological systems. Hence, in this study we synthesized bifunctional nanoparticles, SPIO@SiO_2(FITC) with both fluorescent and magnetic properties, and selected human bone marrow mesenchymal stem cells (hMSCs) as the cell model system. The goal of this research was to develop contrast agent-loaded nanoparticles with which stem cells could be efficiently and harmlessly labeled and then imaged with a clinical MRI analyzer at low cell number.

Bifunctional magnetic iron oxide/silica core−shell nanoparticles with core diameters of 50 and 10 nm were synthesized by a water-in-oil reverse micelle method. Briefly, the monodisperse hydrophobic Fe_3O_4 nanoparticles (10 nm) were synthesized by a seed-growth method by reducing Fe(acac)$_3$ with 1,2-dodecanediol and protected by oleic acid and oleylamine in benzyl ether.[17] After a workup procedure, the Fe_3O_4 nanoparticles were redissolved in cyclohexane at room temperature. Then Triton X-100, hexanol, and H_2O were added with stirring to generate a microemulsion. Then TEOS and N-1-(3-trimethoxysilylpropyl)-N'-fluoresceyl-thiourea (FITC-APTMS) were added to the water-in-oil microemulsion to form the shell structure. The synthesis is based on a sol−gel growth of silica in limited domain of water in the water-in-oil microemulsion. In this way, one can grow an iron oxide (TEM picture in Figure S1) in silica core−shell structure of high uniformity. Details of the syntheses procedure of Fe_3O_4 and SPIO@SiO_2(FITC) are described in Section 1 of the Supporting Information . The nanoparticles were characterized with the transmission electron microscopy (TEM), X-ray powder diffraction pattern (XRD), fluorescence spectroscopy, and T_2 enhancing relaxivity. A TEM image of SPIO@SiO_2(FITC) shows spherical core−shell structure with an average overall size of 50 nm with a 10 nm core (Figure 1). There is a thin ring on the outer surface which may be due to the surface organic group. XRD pattern confirmed the existence of Fe_3O_4 (See Supporting Information, Figure S2). The nanoparticles emit green light with peak at 510 nm. Since the fluorescein dye is in the outer shell away from the iron oxide core, its fluorescence is not quenched significantly by the iron oxide. Dynamic light scattering (DLS) verified that the as-synthesized nanoparticles were homogeneously suspended in the aqueous solution. Because SPIO@SiO_2(FITC) nanoparticles were
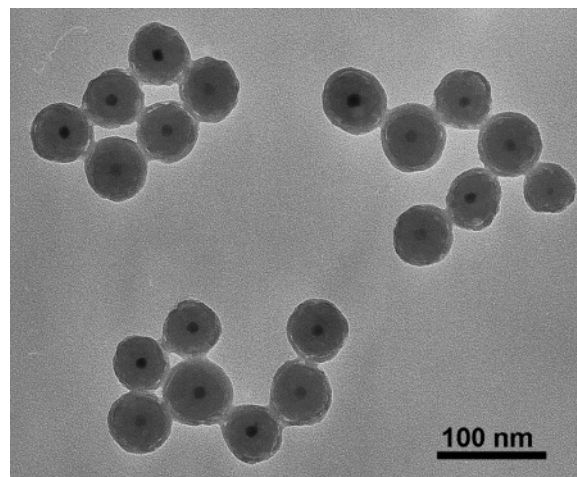

Figure 1. TEM image of SPIO@SiO2(FITC) with an average overall size of 50 nm, 10 nm core, and about 5 nm ring.

well-dispersed in water, the T_2 enhancing capability r_2 (T_2 relaxivity, the slope obtained by plotting $1/T_2$ versus Fe^{3+} content) of SPIO@SiO_2(FITC) could be measured at 0.47 T using a Minispec spectrometer. The relaxivity r_2 is found to be 128 mM^{-1} S^{-1} at 40 °C (Figure S3). The SPIO@SiO_2-(FITC) nanoparticles exhibited the typical property of superparamagnetic iron oxide in shortening T_2 relaxation time.

In the cell-uptake experiments of SPIO@SiO_2(FITC), hMSCs were isolated and expanded (see Supporting Information Section 2) and then incubated with different concentrations of SPIO@SiO_2(FITC) suspension in serum-free low-glucose Dulbecco's modified Eagle's medium (DMEM) for various incubation times. After indicated times, the cells were harvested by trypsinization; cellular uptake of SPIO@SiO_2(FITC) was determined semiquantitatively by the incorporated fluorescence intensity and MR functionalities, using a flow cytometry (Becton Dickenson, Mississauga, CA) and a clinical 1.5-T MRI System (Signa excite, GE Healthcare, USA), respectively (see Supporting Information Section 3). In the flow cytometry data (Figure 2A), the histograms of fluorescence intensity of hMSCs that were incubated with various concentrations of SPIO@SiO_2(FITC) for 1 h were displayed, and data showed that the number of labeled cells and the mean value of fluorescence intensity followed the incubation concentration of SPIO@SiO_2(FITC). We found SPIO@SiO_2(FITC) uptake in hMSCs was time- (30 min, 1, 2, and 4 h) and dose-dependent (3, 10, 30, and 100 μg/mL, see Supporting Information Section 3, Figure S4). The uptake of SPIO@SiO_2(FITC) nanoparticles began significantly as early as 30 min after incubation with 10 μg/mL of nanoparticles and was relatively rapid within the first 1−2 h of incubation. Saturation was achieved at 2 h of incubation in the dose range of 30−100 μg/mL (Figure S4). Using a clinical 1.5-T MRI imager, the MRI images of centrifuged cell pellets in test tubes placed in a water bath were easily detected. Under T2 weighted image mode (T2WI), cells exposed to 30 μg/mL of SPIO@SiO_2(FITC) or higher for 1 h could be easily detected. In Figure 2B, the T2WI of labeled hMSCs showed the MRI signal was dosage dependent. It
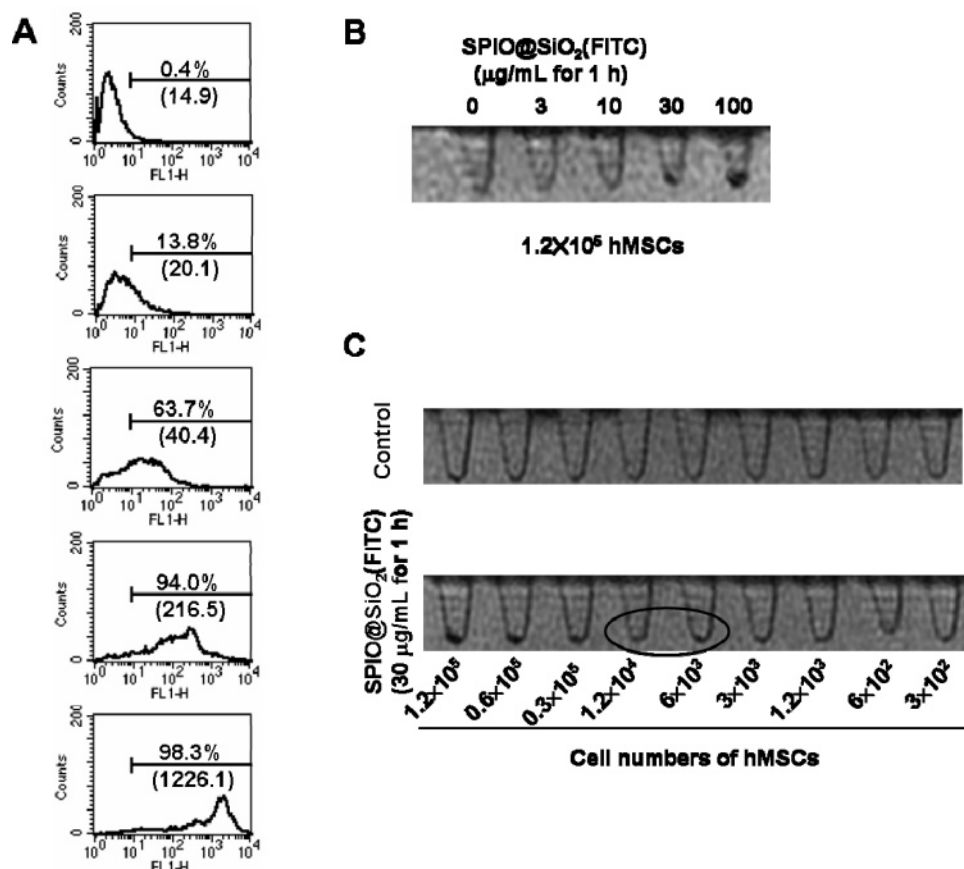
Figure 2. (A) Cellular uptake of SPIO@SiO$_2$(FITC) in hMSCs using flow cytometry. hMSCs were treated with 0 (control), 3, 10, 30, and 100 μg/mL (from top to bottom panels) of SPIO@SiO$_2$(FITC) nanoparticles for 1 h and then immediately processed for flow cytometry study. The mean fluorescence intensity of SPIO@SiO$_2$(FITC)-treated cells is noted in parentheses and the number of positively labeling cells (defined as the fluorescence value $>10^1$) is represented as the percentage of total counting cells in each panel. (B) Representative MRI images of centrifuged hMSCs pellets in Eppendorf tubes placed in a water bath. Each cell pellet contained 1.2 $\times$ 10^5 cells after treatment with various concentrations of SPIO@SiO$_2$(FITC) nanoparticles for 1 h and then scanned under a 1.5-T MRI system. (C) Sensitivity of in vitro MRI of SPIO@SiO$_2$(FITC)-labeled hMSCs. Cells ranging from 3 $\times$ 10^2 to 1.2 $\times$ 10^5 after treatment with 30 μg/mL SPIO@SiO$_2$-(FITC) for 1 h were scanned. Unlabeled cells of identical numbers were scanned as a control group (top panel). The cells could be detected as low signal intensity area which resembles its distribution visualized in the test tube.

also displayed a dose- and time-dependent behavior (Figure S5) as in flow cytometry studies. Hence, for studying the biological effects and the mechanism of SPIO@SiO$_2$(FITC) uptake, an incubation of hMSCs with 30 μg/mL of SPIO@SiO$_2$(FITC) nanoparticles (equal to 0.5 μg iron/mL, see Supporting Information Section 1) for 1 h was chosen. The fact that a small number of hMSCs were easily imaged with a short-term incubation using a clinical 1.5-T MRI analyzer implied the high cellular labeling efficiency of SPIO@SiO$_2$(FITC) nanoparticles. To investigate the limit of labeling, a series of diluted labeled hMSCs were processed for MRI. Figure 2C showed the MR images of SPIO@SiO$_2$-(FITC) nanoparticle-labeled hMSCs could be distinguishably observed at the cell numbers around 10^4. The minimal detecting number of hMSCs is around 6 $\times$ 10^3 to 1.2 $\times$ 10^4. No signal intensity difference could be found in all of the samples in the unlabeled control group.

To evaluate possible cytotoxic effect of SPIO@SiO$_2$(FITC) nanoparticles, cell viability was examined by WST-8 reduction assay (see section 4 of the Supporting Information). No evidence of cytotoxicity was observed at 1 h after treatment with SPIO@SiO$_2$(FITC) nanoparticles, nor was the cell proliferation affected after SPIO@SiO$_2$(FITC) nanoparticle-treated cells were incubated with growth medium for 24 h (see Figure 3A). In addition, we examined the differentiation potential of labeled hMSCs into adipocytes and osteocytes to examine possible adverse effects of SPIO@SiO$_2$(FITC) nanoparticles on the functions of stem cells. Adipogenic differentiation with the formation and accumulation of lipid vacuoles and osteogenic differentiation with alkaline phosphatase activity were observed by oil-red O stain and Fast Blue stain (Sigma-Aldrich), respectively (see section 4 of the Supporting Information). As shown in Figure 3B, adipogenic differentiation of hMSCs was observed only in cells grown in adipogenic medium but not in regular growth medium. SPIO@SiO$_2$(FITC) nanoparticle-treated hMSCs did differentiate into adipocytes, and there was no obvious difference in oil-red O stain assay between SPIO@SiO$_2$-(FITC) nanoparticle-treated control cells and untreated control cells. Figure 3C shows that SPIO@SiO$_2$(FITC) nanoparticles did not affect the osteogenic differentiation induced by incubating hMSCs with osteogenic medium. These data indicated that SPIO@SiO$_2$(FITC) nanoparticles were biocompatible. Moreover, after incubation with different
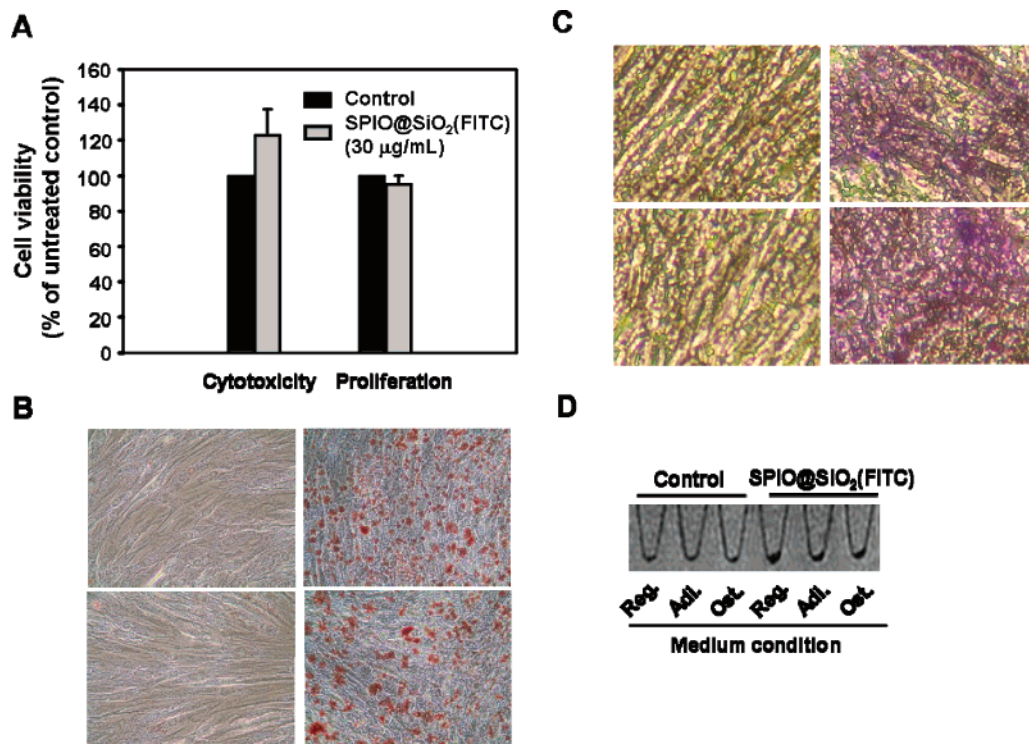
Figure 3. (A) hMSCs were incubated in the absence (control) or presence of 30 μg/mL SPIO@SiO2(FITC) for 1 h. Cytotoxicity of SPIO@SiO$_2$(FITC) was determined using a CCK-8 assay immediately after 1 h of incubation (the left two bars). The effect of SPIO@SiO$_2$-(FITC) on cell proliferation was examined after hMSCs were allowed to grow in regular growth medium for 24 h after 1 h of incubation with SPIO@SiO$_2$(FITC) (the right two bars). Data are expressed as mean $\pm$ standard error of three determinations (each in quadruplicate). Effects of SPIO@SiO$_2$(FITC) on adipogenic (B) and osteogenic (C) differentiation of hMSCs. Cells were first treated with vehicle (top panels in each figure) or 30 μg/mL SPIO@SiO$_2$(FITC) (bottom panels in each figure) for 1 h and then incubated with regular growth medium as negative control (left panels in each figure), adipogenic medium (right panels in Figure B), or osteogenic medium (right panels in part C) for differentiation. Original magnification, $\times$200. The images represent three independent experiments. (D) hMSCs were first incubated in the absence (control) or presence of 30 μg/mL SPIO@SiO$_2$(FITC) for 1 h, and then cells were incubated with regular growth medium (Reg.), adipogenic medium (Adi.), and Osteogenic medium (Ost.), for 7 days. After incubation, cells were harvested, processed, and scanned under a 1.5-T MRI system. T2WI showed there are significantly different signal intensities for the treated cells from control.

media for 7 days, the cells prelabeled with SPIO@SiO$_2$-(FITC) nanoparticles for 1 h still could be detected under T2WI in a clinical 1.5-T MRI imager (see Figure 3D).

Endocytosis is known as the main mechanism of cellular internalization for the magnetic nanoparticle vectors. Since SPIO@SiO$_2$(FITC) nanoparticles could be efficiently internalized into hMSCs, we used various pharmacological inhibitors to explore the underlying uptake mechanism. Flow cytometry data showed that SPIO@SiO$_2$(FITC) uptake was impeded by phenylarsine oxide (PAO; a clathrin inhibitor) and cytochalasin D (CytD; an actin inhibitor) but not by filipin (a caveola inhibitor) nor nocodazole (Noco; a microtubule inhibitor) (see Figure 4A). Similar inhibitory effects of these inhibitors on SPIO@SiO$_2$(FITC) uptake were verified by MRI. To improve the MRI sensitivity, 2.4×10^5 cells were processed for comparison under T2WI. As shown in Figure 4B, SPIO@SiO$_2$(FITC)-labeled cells treated with PAO or CytD exhibited lower signal intensity, which indicated inhibition of particle uptake by these inhibitors. These indicated that clathrin-coated pit endocytosis and actin microfilaments might be involved in controlling the highly efficient intracellular uptake of SPIO@SiO$_2$(FITC) nanoparticles. In order to find out if the ingested particles are delivered to early endosomes and then (via late endosomes)

to lysosomes after endocytosis, we studied the colocalization of LysoTracker Red, a marker for late endosomes and lysosomes with red fluorescence, with SPIO@SiO$_2$(FITC) nanoparticles (green fluorescence). In the meanwhile, to avoid the artifact of cytochemical fixing, live cells after incubation with SPIO@SiO$_2$(FITC) nanoparticles and LysoTracker Red were visualized with a Zeiss Axiovert 100 M confocal unit (see section 6 of the Supporting Information). Indeed, SPIO@SiO$_2$(FITC) nanoparticles could be internalized into hMSCs via endocytosis which was evidenced by colocalization of LysoTracker Red and SPIO@SiO$_2$-(FITC) nanoparticles in late endosomes and lysosomes as exhibiting the orange to yellow fluorescence (see Figure 4C).

Finally, we conducted MRI images of SPIO@SiO$_2$(FITC)-labeled hMSCs in a nude mice model. Either 1.2×10^4 or 1.2×10^5 hMSCs treated with 30 μg/mL of SPIO@SiO$_2$-(FITC) nanoparticles for 1 h were suspended in 10 μL of Matrigel and injected subcutaneously and separately into the dorsal flanks of each nude mouse (Figure 5). Under T2WI, hMSCs labeled with SPIO@SiO$_2$(FITC) (1.2×10^5 hMSCs) could be detected in a 1.5-T MRI at the dorsal flanks of the nude mouse and presented as a dark, protruding mass mimicking a subcutaneous tumor, while the 1.2×10^4 labeled hMSCs could only be detected as a bright dot, a signal which
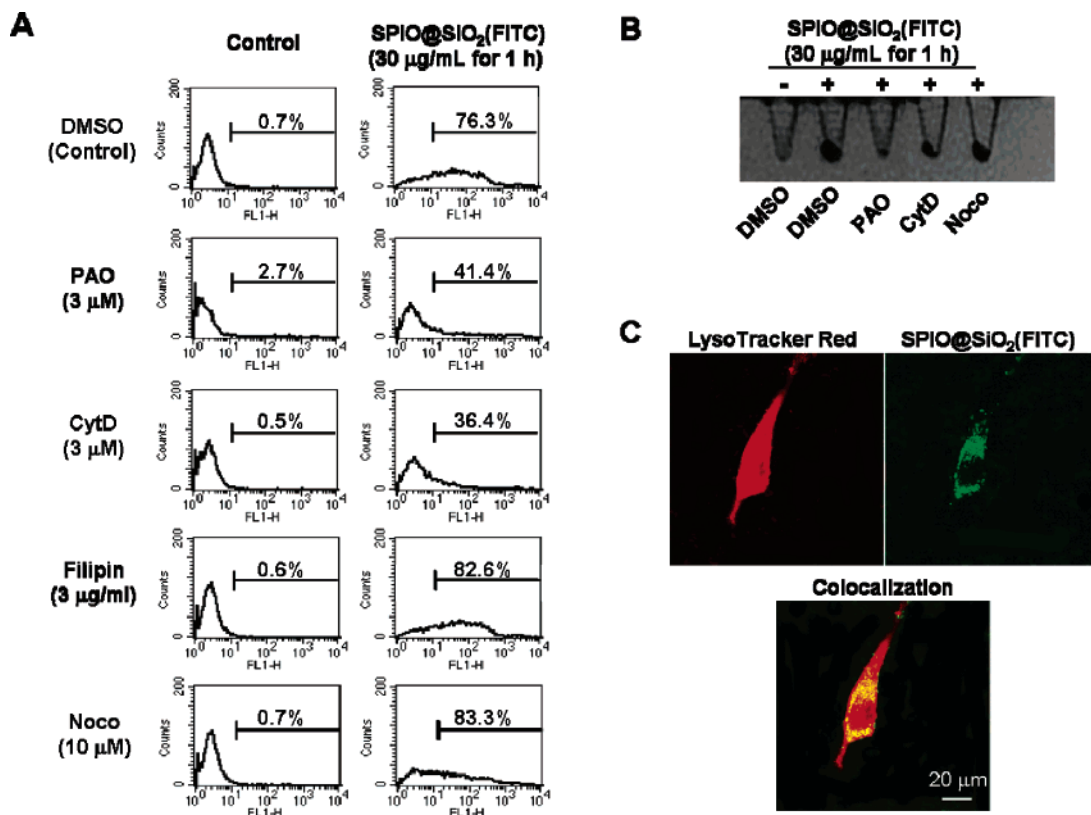
Figure 4. Effects of various inhibitors on the uptake of SPIO@SiO$_2$(FITC). (A) hMSCs were treated with a vehicle (DMSO, control) or the indicated inhibitors in the absence (left panels as negative control) or presence of 30 μg/mL SPIO@SiO$_2$(FITC) (right panels) for 1 h. After treatment, uptake was detected by flow cytometry. The number of positively labeling cells is represented as the percentage of total counting cells in each panel. (B) The internalization mechanism of SPIO@SiO$_2$(FITC) was further evidenced by MRI. SPIO@SiO$_2$(FITC)-labeled cells treated or untreated with various inhibitors were scanned at identical cell number, 2.4×10^5. (C) Colocalization of green fluorescent SPIO@SiO$_2$(FITC) with late endosomes/lysosomes. hMSCs were treated with 30 μg/mL SPIO@SiO$_2$(FITC) for 30 min and then incubated with LyosTracker Red for another 30 min. The cellular distribution of SPIO@SiO$_2$(FITC) and LysoTracker Red-labeled organelles (late endosomes/lysosomes) was analyzed by a Zeiss Axiovert 100M confocal unit.
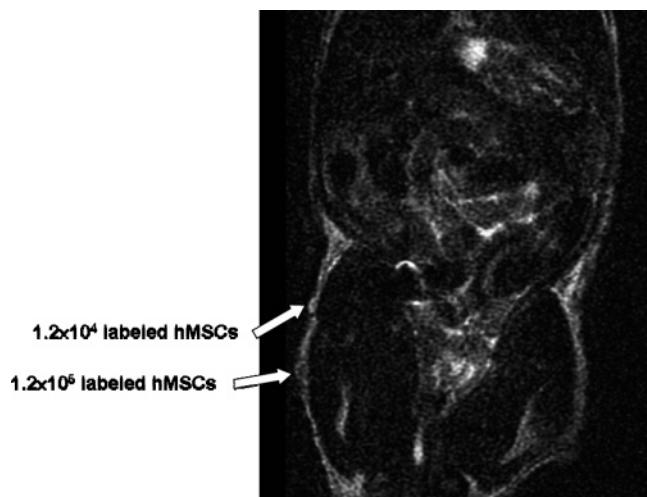

Figure 5. T2 weighted MRI study of SPIO@SiO$_2$(FITC)-labeled hMSCs was performed by injecting 1.2×10^4 or 1.2×10^5 cells mixed with Matrigel into subcutaneous tissue of the flanks (unlabeled cells at left flank and labeled cells at right flank, respectively) of a nude mouse.

only reflects Matrigel. The findings revealed that labeled cells could be detected in a dose-responsive manner in living animals under a clinical MRI system.

In this study, we have demonstrated that our as-synthesized SPIO@SiO$_2$(FITC) nanoparticles could be efficiently internalized into hMSCs. The improvements we have achieved are as follows: (1) the procedure used to label hMSCs is fast (only 30 min to 1 h of incubation) and easy to apply; (2) the concentration of SPIO@SiO$_2$(FITC) nanoparticles for labeling cells is low; (3) these labeled cells can be visualized in a clinical 1.5-T MRI imager with an in vivo detecting quantity of 1.2×10^5 cells and with detectable cell numbers about 10^4 in vitro; (4) the distinguishability of labeled hMSCs under a clinical MRI imager is high in vivo. Moreover, SPIO@SiO$_2$(FITC) nanoparticles are nontoxic without affecting cell viability, growth, and differentiation of hMSCs. The labeled cells remained MRI detectable after long-term (7 days) growth or differentiation, which is further evidence for the biocompatibility and durability of SPIO@SiO$_2$(FITC) nanoparticles. In summary, although further investigations and an alternative animal model of stem cell transplantation are warranted to evaluate potential applications for stem cell tracking, our results strongly suggest SPIO@SiO$_2$(FITC) nanoparticles are a superior multifunctional tracking agent.

094-PP-02 and NM-095-PP-02) Taiwan, and from the National Science Council (NSC 95-2120-M-002-009) of Taiwan.

Supporting Information Available: A detailed description of the experimental procedures and of the materials used. This material is available free of charge via the Internet at http://pubs.acs.org.

References

(1) Bulte, J. W.; Douglas, T.; Witwer, B.; Zhang S. C.; Lewis, B. K.; van Gelderen, P.; Zywicke, H.; Duncan, I. D.; Frank, J. A. *Acad. Radiol.* **2002**, *9* (Suppl 2), S332−S335.
(2) Bulte, J. W.; Duncan, I. D.; Frank, J. A. *J. Cereb. Blood Flow Metab.* **2002**, *22*, 899−907.
(3) Bulte, J. W.; Kraitchman, D. L. *NMR Biomed.* **2004**, *17*, 484−499.
(4) Lewin, M.; Carlesso, N.; Tung, C. H.; Tang, X. W.; Cory, D.; Scadden, D. T.; Weissleder, R. *Nat. Biotechnol.* **2000**, *18*, 410−414.
(5) Hill, J. M.; Dick, A. J.; Raman, V. K.; Thompson, R. B.; Yu, Z. X.; Hinds, K. A.; Pessanha, B. S.; Guttman, M. A.; Varney, T. R.; Martin, B. J.; Dunbar, C. E.; McVeigh, E. R.; Lederman, R. J. *Circulation* **2003**, *108*, 1009−1014.
(6) Bulte, J. W.; Douglas, T.; Witwer, B.; Zhang, S. C.; Strable, E.; Lewis, B. K.; Zywicke, H.; Miller, B.; van Gelderen, P.; Moskowitz, B. M.; Duncan, I. D.; Frank, J. A. *Nat. Biotechnol.* **2001**, *19*, 1141−1147.
(7) Rudelius, M.; Daldrup-Link, H. E.; Heinzmann, U.; Piontek, G.; Settles, M.; Link, T. M.; Schlegel, J. *Eur. J. Nucl. Med. Mol. Imaging* **2003**, *30*, 1038−1044.
(8) Jendelová, P.; Herynek, V.; DeCroos, J.; Glogarova, K.; Andersson, B.; Hájek, M.; Syková, E. *Magn. Reson. Med.* **2003**, *50*, 767−776.
(9) Jendelová, P.; Herynek, V.; Urdzíková, L.; Glogarová, K.; Kroupová, J.; Andersson, B.; Bryja, V.; Burian, M.; Hájek, M.; Syková, E. *J. Neurosci. Res.* **2004**, *76*, 232−243.
(10) Daldrup-Link, H. E.; Rudelius, M.; Oostendorp, R. A.; Settles, M.; Piontek, G.; Metz, S.; Rosenbrock, H.; Keller, U.; Heinzmann, U.; Rummeny, E. J.; Schlegel, J.; Link, T. M. *Radiology* **2003**, *228*, 760−767.
(11) Daldrup-Link, H. E.; Rudelius, M.; Piontek, G.; Metz, S.; Brauer, R.; Debus, G.; Corot, C.; Schlegel, J.; Link, T. M.; Peschel, C.; Rummeny, E. J.; Oostendorp, R. A. *Radiology* **2005**, *234*, 197−205.
(12) Ju, S.; Teng, G.; Zhang, Y.; Ma, M.; Chen, F.; Ni, Y. *Magn. Reson. Imaging* **2006**, *24*, 611−617.
(13) Mulder, W. J. M.; Koole, R.; Brandwijk, R. J.; Storm, G.; Chin, P. T. K.; Strijkers, G. J.; Donega, C. D. M.; Nicolay, K.; Griffioen, A. W. *Nano Lett.* **2006**, *6*, 1−6.
(14) Huh, Y. M.; Jun, Y. W.; Song, H. T.; Kim, S.; Choi, J. S.; Lee, J. H.; Yoon, S.; Kim, K. S.; Shin, J. S.; Suh, J. S.; Cheon, J. *J. Am. Chem. Soc.* **2005**, *127*, 12387−12391.
(15) Yonn, T. J.; Kim, J. S.; Kim, B. G.; Yu, K. N.; Cho, M. H.; Lee, J. K. *Angew. Chem., Int. Ed.* **2005**, *44*, 1068−1071.
(16) Huang, D. M.; Hung, Y.; Ko, B. S.; Hsu, S. C.; Chen, W. H.; Chien, C. L.; Tsai, C. P.; Kuo, C. T.; Kang, J. C.; Yang, C. S.; Mou, C. Y.; Chen, Y. C. *FASEB J.* **2005**, *19*, 2014−2016.
(17) Sun, S.; Zeng, H. *J. Am. Chem. Soc.* **2002**, *124*, 8204−8205.

NL0624263